ARMY RESEARCH LABORATORY

Computer Simulations: A Tool to Predict Experimental Parameters with Cold Atoms

by Violeta Prieto, Jason Alexander, Christopher Rowlett, William Golding, and Patricia Lee

ARL-TR-6420 **April 2013**

NOTICES

Disclaimers

The findings in this report are not to be construed as an official Department of the Army position unless so designated by other authorized documents.

Citation of manufacturer's or trade names does not constitute an official endorsement or approval of the use thereof.

Destroy this report when it is no longer needed. Do not return it to the originator.

Army Research Laboratory
Adelphi, MD 20783-1197

ARL-TR-6420 **April 2013**

Computer Simulations: A Tool to Predict Experimental Parameters with Cold Atoms

Violeta Prieto, Jason Alexander, Christopher Rowlett, William Golding, and Patricia Lee
Sensors and Electron Devices Directorate, ARL

REPORT DOCUMENTATION PAGE

Form Approved
OMB No. 0704-0188

1. REPORT DATE *(DD-MM-YYYY)*	2. REPORT TYPE	3. DATES COVERED (From - To)
April 2013	Final	

4. TITLE AND SUBTITLE
Computer Simulations: A Tool to Predict Experimental Parameters with Cold Atoms

5a. CONTRACT NUMBER
W911QX-04-C-0129

5b. GRANT NUMBER

5c. PROGRAM ELEMENT NUMBER

6. AUTHOR(S)
Violeta Prieto, Jason Alexander, Christopher Rowlett, William Golding, and Patricia Lee

5d. PROJECT NUMBER

5e. TASK NUMBER

5f. WORK UNIT NUMBER

7. PERFORMING ORGANIZATION NAME(S) AND ADDRESS(ES)
U.S. Army Research Laboratory
ATTN: RDRL-SEE-I
2800 Powder Mill Road
Adelphi, MD 20783-1197

8. PERFORMING ORGANIZATION REPORT NUMBER
ARL-TR-6420

9. SPONSORING/MONITORING AGENCY NAME(S) AND ADDRESS(ES)

10. SPONSOR/MONITOR'S ACRONYM(S)

11. SPONSOR/MONITOR'S REPORT NUMBER(S)

12. DISTRIBUTION/AVAILABILITY STATEMENT
Approved for public release; distribution unlimited.

13. SUPPLEMENTARY NOTES

14. ABSTRACT
Computer simulations are commonly used in the laboratory to support, facilitate, or optimize the experimental process. We present the use of two different software packages, COMSOL and LiveAtom, and explain how they assist us through the experimental procedure. Both programs perform finite element analysis to solve partial differential equations. COMSOL is a multiphysics simulation software that is very powerful and particularly useful for solving and visualizing physical problems. LiveAtom was specifically designed to work with cold atom systems and atom chips, and is already able to compute their key properties. We simulate our experimental parameters by combining the results of the two programs.

15. SUBJECT TERMS
COMSOL, LiveAtom, simulation, atom chip

16. SECURITY CLASSIFICATION OF:			17. LIMITATION OF ABSTRACT	18. NUMBER OF PAGES	19a. NAME OF RESPONSIBLE PERSON
a. REPORT	b. ABSTRACT	c. THIS PAGE			Violeta Prieto
Unclassified	Unclassified	Unclassified	UU	30	19b. TELEPHONE NUMBER (*Include area code*) (301) 394-2119

Standard Form 298 (Rev. 8/98)
Prescribed by ANSI Std. Z39.18

Contents

List of Figures

1. Introduction

This report provides an overview of computer simulations using two different software packages, COMSOL (*1*) and LiveAtom (*2*), and how we use them to predict experimental parameters. COMSOL is a multiphysics simulation software that allows modeling by defining the geometry, specifying the meshing and the physics, solving the problem, and then visualizing the results. It uses general predefined multiphysics for the most common problem types, but also allows one to choose different physics and define the interdependencies between them. It is not specifically designed for cold atom systems or atom chips, the physics has to be programmed by hand, but it is very versatile. It can be very valuable when looking for electromagnetic and radio frequency (RF) effects, in estimating and predicting potential thermal issues, as well as in designing new chips. COMSOL has over 20 different modules that allow the use of different physics. It uses two types of solvers: direct and iterative. Direct solvers are very robust, but scale poorly with problem size, especially for three-dimensional (3D) problems. Iterative solvers avoid different types of operations such as matrix inversion; they can be very fast and use relatively little memory, but the selection can be very problem dependent. For the simulations shown in this report, we use the AC/DC module and the "Electric Currents" and "Magnetic Fields" physics. We first define the current flowing through the wires by selecting the boundary terminals and choosing the corresponding current. This allows us to calculate the current density by using the current conservation, electric insulation, and initial values of the electrical potential. To compute the magnetic field, we set up a stationary problem with an external current density and a null magnetic vector potential and use Ampere's Law by taking into account the boundary conditions of the problem.

On the other hand, LiveAtom was specifically designed for cold atoms and atom chips. It only allows one-dimensional (1D) and two-dimensional (2D) wire configurations; however, since the wires in general are very thin, this is usually a good approximation. LiveAtom first determines the current density distribution due to the 1D or 2D wire configuration and then uses direct integration (Biot-Savart law) to calculate the magnetic field. For the 2D wires, it uses finite element analysis to find the current distribution and adaptive mesh refinement to minimize the computation time. With LiveAtom, it is possible to visualize the magnetic fields due to a given 1D or 2D wire configuration in three dimensions and find the corresponding traps, allowing us to look at the trap frequency, depth, and axes. It can also simulate the atom behavior using Monte Carlo simulations. Since the computation server is hosted "in the cloud," the simulations benefit from the power and speed of cluster type computing.

It is the Army's goal to build precise inertial sensors (*3*). These can be used in navigation, to detect underground structures, as well as to accomplish non-intrusive measurement of mass distribution within closed containers. We are working toward building a small, portable inertial

sensor by using atom chip technology and cold atom interferometry (*4–8*). Atom chips allow the miniaturization and potential portability of the device by implementing complex technologies such as mirrors, beam splitters, waveguides, and gratings into tight spaces (*9–11*). Coherent splitting with a well-defined, repeatable relative phase is a requirement for cold atom interferometry. We use computer simulations to model the dynamical splitting of the atom cloud to create an interferometer by combining different current configurations with various external bias fields.

The cold atom system we use was developed by Cold Quanta (*12,13*). Figure 1 depicts the system and associated optics. Our system consists of two chambers separated by a silicon disk with a 750-µm hole drilled into it. The lower chamber is labeled 2D magneto-optical trap (MOT) and is surrounded by four coils (visible) to provide the magnetic confinement. The upper chamber, labeled three-dimensional (3D) MOT is surrounded by six coils (not shown in the picture) to provide magnetic confinement and translation. Our atom chip sits on top of the upper chamber. The external Z wire (not shown in the picture) is positioned above the upper chamber. Figure 2 shows the upper chamber with the coils and the external Z wire on the left and the part of the external Z wire facing the cell on the right. Figure 3 is an overview of our experimental procedure. We release hot rubidium (Rb) atoms (just slightly above room temperature) into the lower chamber. The atoms are cooled in a 2D MOT and form a collimated atomic beam. The 2D MOT is unconfined in the vertical direction and a laser beam pushes the atoms through the hole to the upper chamber. Reflection of the beam off the silicon disk provides additional cooling in the lower chamber. The atoms are captured in a 3D MOT and then compressed to a compressed MOT (CMOT) by ramping up the fields and detuning the lasers from resonance. Then an external Z wire catches the atoms and moves them from the center of the upper chamber (about 14 mm from the chip) to about 200 µm from the chip. We then turn the atom chip while turning off the external Z wire on and cool further to Bose-Einstein condensation (BEC). Once captured on the chip, we perform designed experiments. A much more detailed description of our setup and experimental procedure is provided in reference 14.

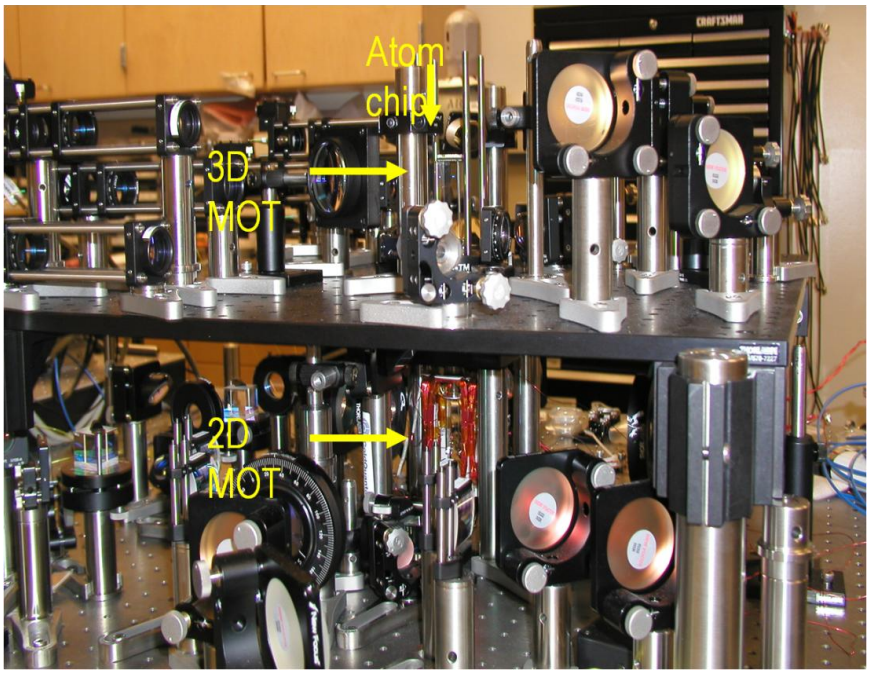

Figure 1. Two-chamber system and associated optics. The 3D MOT coils have been removed to provide visual access to the upper chamber.

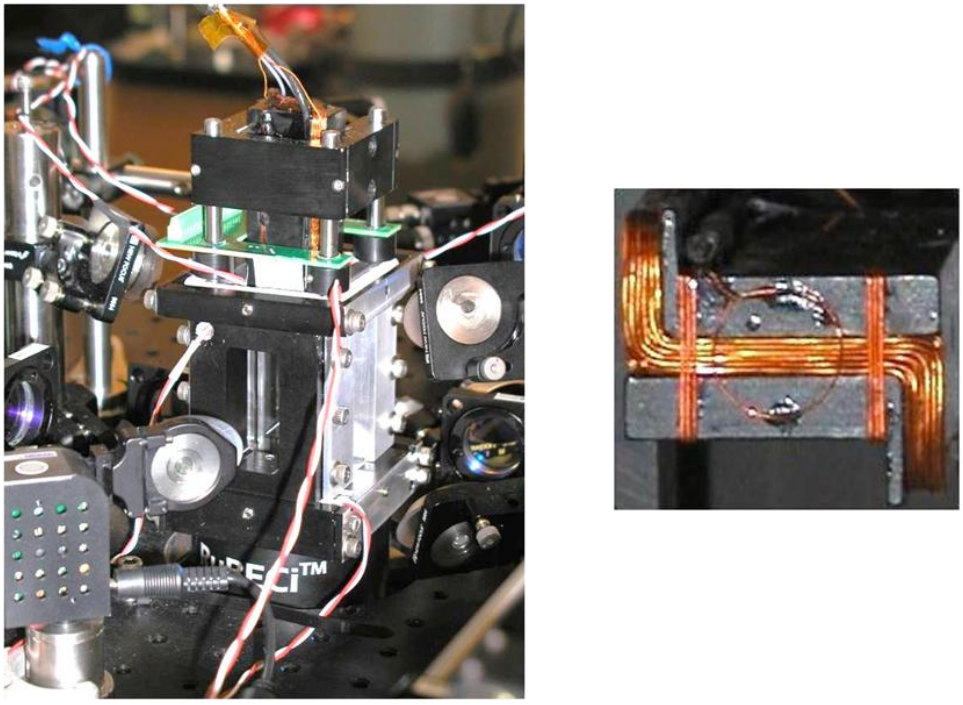

Figure 2. Upper chamber with all the coils in place (left) and view of the external Z wire facing the cell (right).

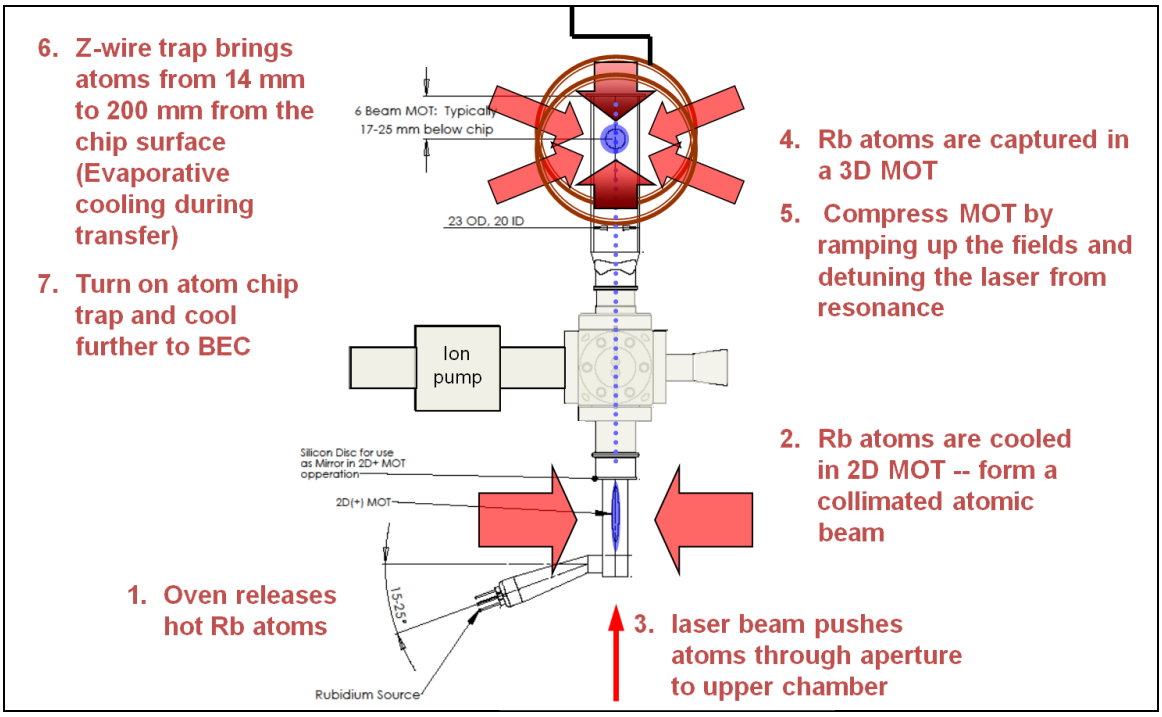

Figure 3. Experimental procedure overview.

In this report, we show the simulations of the current configurations and magnetic fields produced by the different coils in the upper chamber of our system. Then, we show the current configurations and magnetic fields used in our atom chip and explore different outcomes that can be achieved with specific current configurations. Finally, we present exotic geometries that have potentially interesting applications.

2. Magnetic Fields Produced by Coils

The vacuum chamber is surrounded by three pairs of coils: the Bx coils, By coils, and Bz coils. Figure 4 shows the overall construction and location of the coils, as well as the external Z wire and the atom chip at the top of the chamber. The coil structure is about 2 in^2 by about 3.4 inches in height. Ideally, the coils would be large enough to produce a uniform magnetic field in the region of interest. However, since this is not the case, we model the field produced by the different coils inside the vacuum chamber. In this section, we present the results for the x, y, and z bias fields (in Helmholtz configuration), as well as for the By coils in anti-Helmholtz configuration and due to our external Z wire. The simulations are verified with both COMSOL and LiveAtom and are presented in COMSOL.

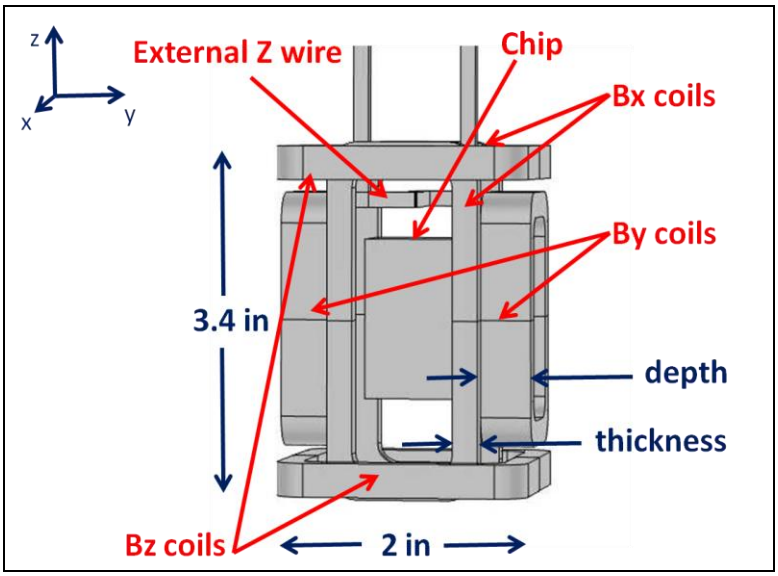

Figure 4. Coil locations, upper chamber.

2.1 Bx Field

The x bias field is produced by the x bias coils. Each of them consists of 100 turns of 23 gauge wire with external dimensions of 3.5 in long by 1.5 in wide by 0.25 in thick by 0.25 in deep. The coils are located in the yz plane at x= ± 0.875 in. For a 1-A current stored in each of the x bias coils (counterclockwise in the yz plane), the magnetic field points in the +x direction. Figure 5 shows the magnitude and direction of the magnetic field due to the abovementioned current in the yz plane at x = 0. The magnetic field ranges between 14 and 19 G. Figure 6 shows the magnitude of the field in the xz plane at y = 0. The magnetic field ranges between 19 and 25 G. Note that the magnetic field at the center is about 19 G consistently in both figures 5 and 6.

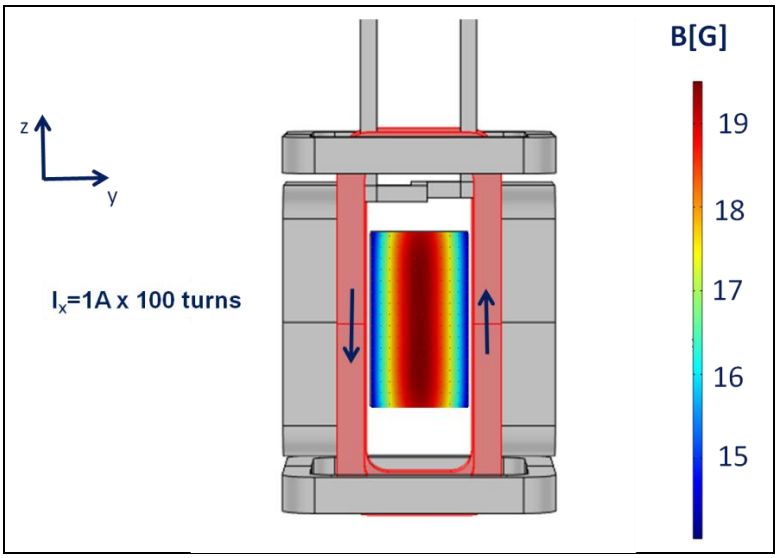

Figure 5. Magnitude and direction of the magnetic field due to a 1-A current stored (counterclockwise in the yz plane) in each of the x bias coils

(highlighted in red) as seen at x = 0 in the yz plane.

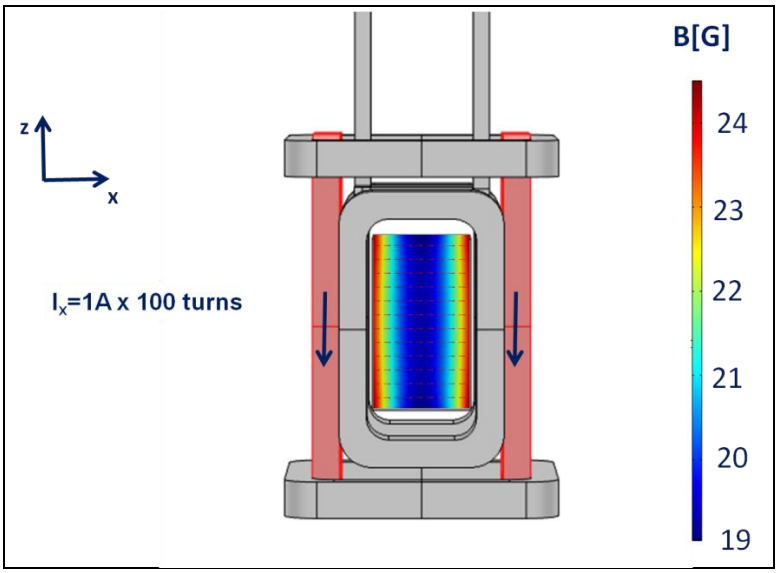

Figure 6. Magnitude and direction of the magnetic field due to a 1-A current stored (counterclockwise in the yz plane) in each of the x bias coils (highlighted in red) as seen at y = 0 in the xz plane.

2.2 By Field

We operate the y coils to produce a y bias and the MOT field. Each of the y coils consists of 225 turns of 23 gauge wire with external dimensions of 2.5 in long by 1.5 in wide by 0.25 in thick by 0.5 in deep. They are located in the xz plane at y= ± 1 in. The y bias field is produced by the y bias coils in Helmholtz configuration. For a 1-A current stored in each of the y bias coils (clockwise in the xz plane), the magnetic field points in the +y direction. Figure 7 shows the magnitude and direction of the magnetic field due to the abovementioned current in the xz plane at y = 0. The magnetic field ranges between 20 and 38 G. Figure 8 shows the magnitude of the field in the yz plane at x = 0. The magnetic field ranges between 27 and 50 G. Note that the magnetic field at the center is about 37 G consistently in both figures 7 and 8.

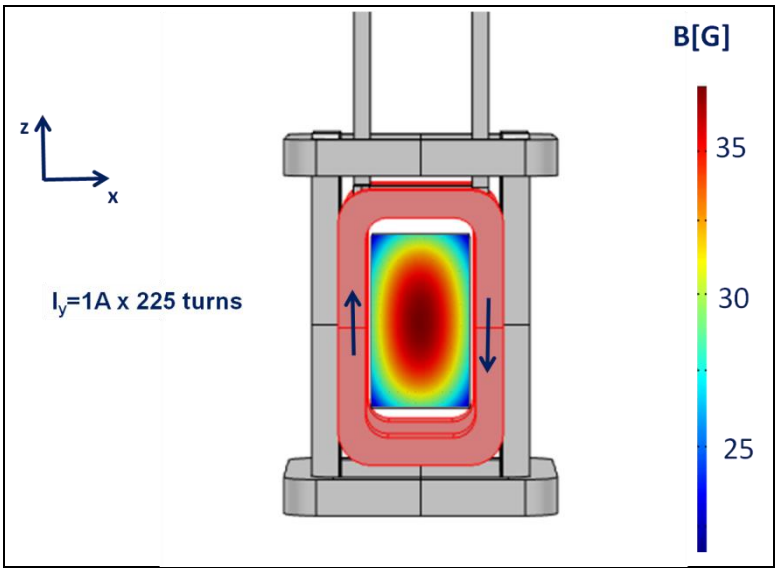

Figure 7. Magnitude and direction of the magnetic field due to a 1-A current stored (clockwise in the xz plane) in each of the y bias coils (highlighted in red) as seen in at y = 0 the xz plane.

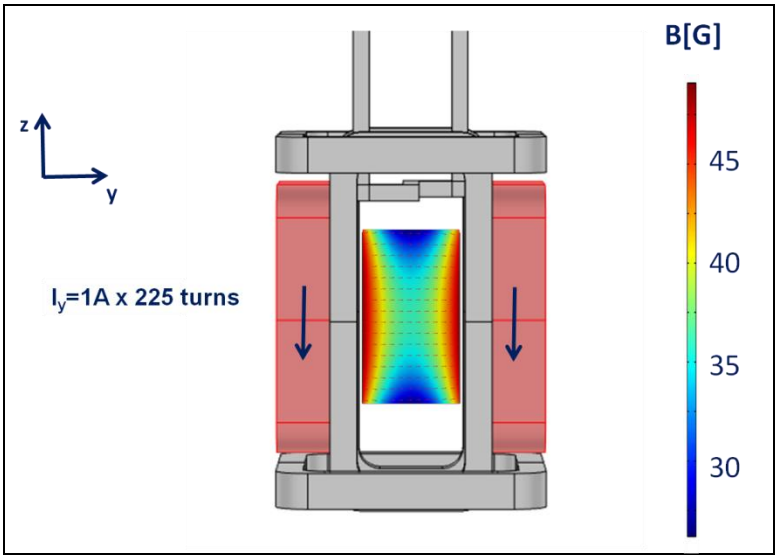

Figure 8. Magnitude and direction of the magnetic field due to a 1-A current stored (clockwise in the xz plane) in each of the y bias coils (highlighted in red) as seen at x = 0 in the yz plane.

2.3 Bz Field

The z bias field is produced by the z bias coils. Each of them consists of 150 turns of 23 gauge wire with external dimensions of 2.5 in long by 2.5 in wide by 0.25 in thick by 0.33 in deep. The coils are located in the xy plane at z= ± 1.545 in. For a 1-A current stored in each of the z bias coils (counterclockwise in the xy plane), the magnetic field points in the +z direction. Figure 9 shows the magnitude and direction of the magnetic field due to the abovementioned current in

the yz plane at x = 0. The magnetic field ranges between 12 and 22 G. Figure 10 shows the magnitude of the field in the xz plane at y = 0. Since these coils are squares, the field seen in the xz plane is the same as in the yz plane.

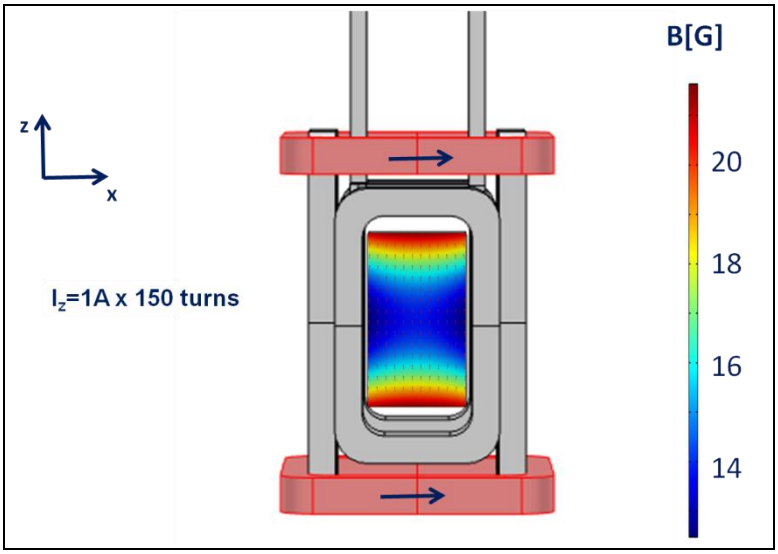

Figure 9. Magnitude and direction of the magnetic field due to a 1-A current stored (counterclockwise in the xy plane) in each of the z bias coils (highlighted in red) as seen at x = 0 in the yz plane.

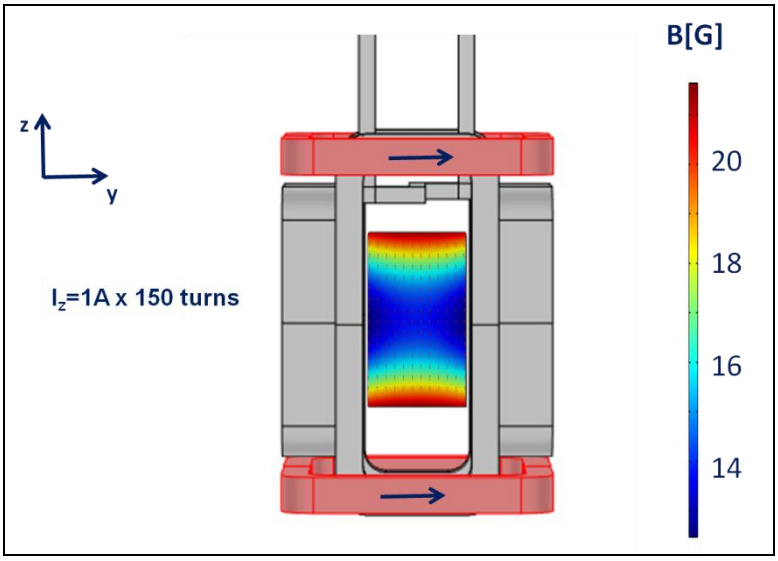

Figure 10. Magnitude and direction of the magnetic field due to a 1-A current stored (counterclockwise in the xy plane) in each of the z bias coils (highlighted in red) as seen at y = 0 in the xz plane.

2.4 MOT Field

As mentioned before, we operate the y coils to produce a y bias and the MOT field. The MOT field is produced by the y bias coils in anti-Helmholtz configuration by storing current

counterclockwise in the coil located at y = 1 in and clockwise in the one located at y = –1 in, as seen in the xz plane. For a 1-A current stored in each of the y bias coils in this configuration, figure 11 shows the magnitude and direction of the magnetic field in the xz plane at y = 0, while figure 12 shows the magnitude of the field in the yz plane at x = 0. In both figures, the field minimum corresponds to the center of the coils, where we trap our initial MOT.

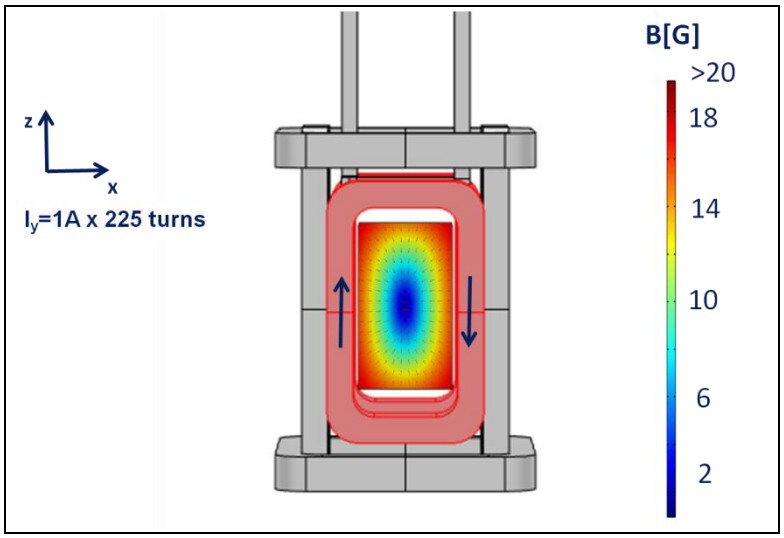

Figure 11. Magnitude and direction of the magnetic field due to a 1-A current stored in each of the y bias coils (highlighted in red) in anti-Helmholtz configuration with current stored counterclockwise in the coil located at y = 1 in and clockwise in the one located at y = –1 in as seen at y = 0 in the xz plane.

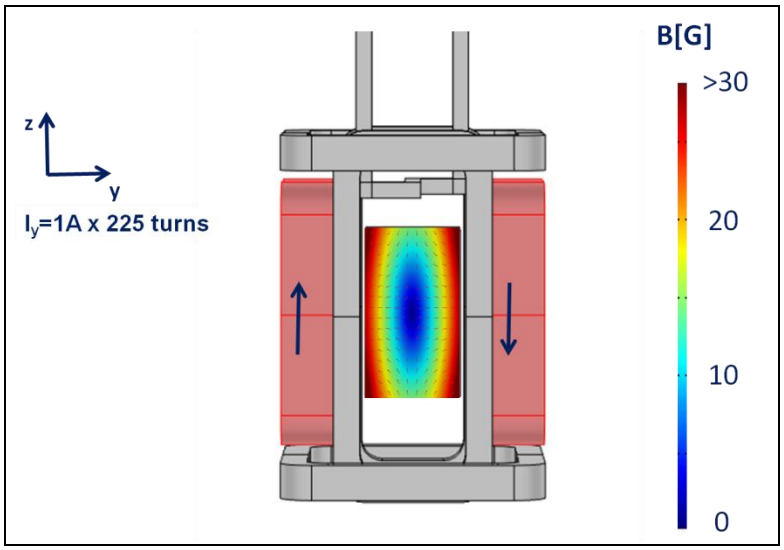

Figure 12. Magnitude and direction of the magnetic field due to 1 A current stored in each of the y bias coils (highlighted in red) in anti-Helmholtz configuration with current stored counterclockwise in the coil located at y= 1 in and clockwise in the one located at y= –1 in as seen at x = 0 in the yz plane.

As part of our experimental procedure, we move our trap bottom by applying a z bias magnetic field. The effect of adding a Bz = 0.75 G is seen at y = 0 in the xz plane in figure 13 and at x = 0 in the yz plane in figure 14.

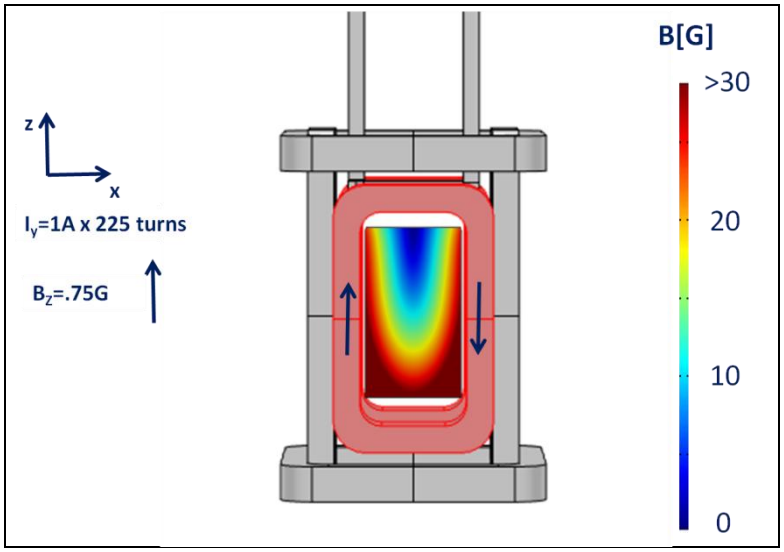

Figure 13. Magnitude and direction of the magnetic field due to a 1-A current stored in each of the y bias coils (highlighted in red) in anti-Helmholtz configuration with current stored counterclockwise in the coil located at y = 1 in and clockwise in the one located at y = –1 in as seen in the xz plane at y = 0 and a z bias field of 0.75G.

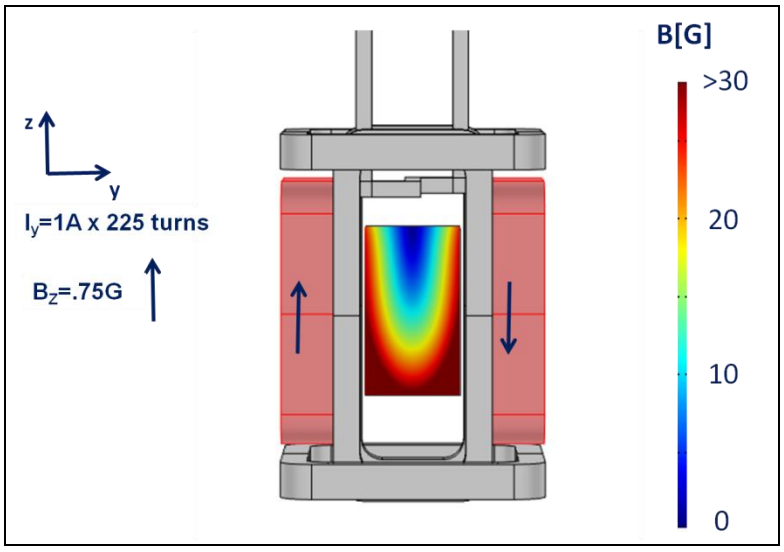

Figure 14. Magnitude and direction of the magnetic field due to a 1-A current stored in each of the y bias coils (highlighted in red) in anti-Helmholtz configuration with current stored counterclockwise in the coil located at y = 1 in and clockwise in the one located at y = –1 in as seen in the yz plane at x = 0 and a z bias field of 0.75G

2.5 External Z Wire

The external Z wire has a Z shape that is 1.25 in long by 1.1 in wide by 0.15 in thick by 0.15 in deep, and consists of 36 turns of 23 gauge wire. After trapping the atoms in the MOT and moving them up, we capture them with the external Z wire. In order to obtain a successful transfer, we match the location of the trap bottom of the two configurations. Figures 15 and 16 show the magnetic trap obtained with 20 A in the external Z wire, Bx = 10 G, and By = 25 G as seen at x = 0 in the yz plane and at y = 0 in the xz plane, respectively.

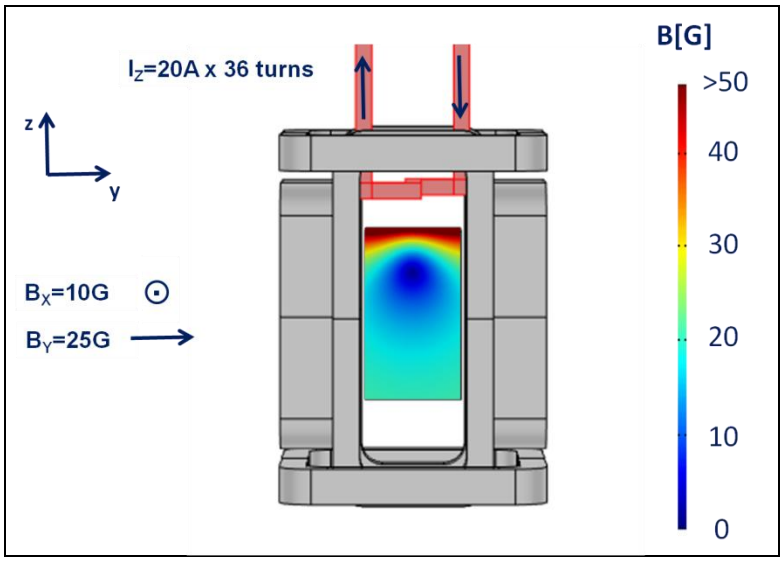

Figure 15. Magnetic field produced with a 20-A current stored in the external Z wire, Bx = 10 G, and By = 25 G as seen at x = 0 in the yz plane.

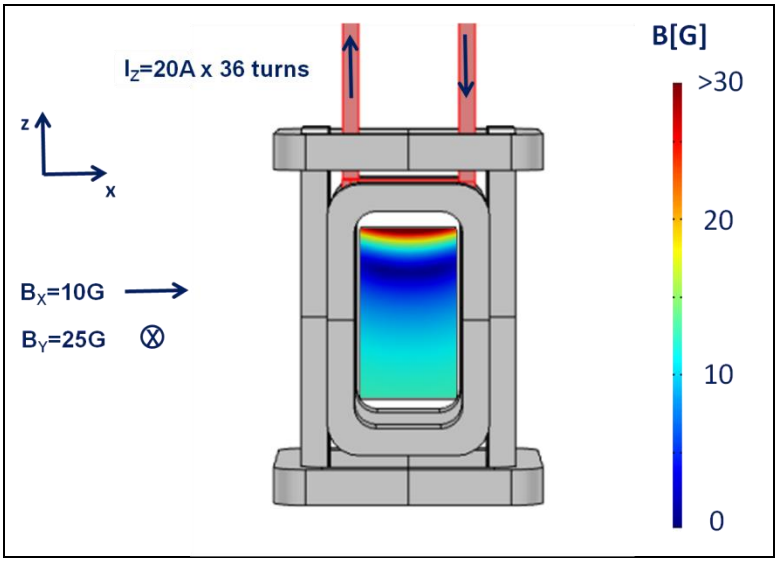

Figure 16. Magnetic field produced with a 20-A current stored in the external Z wire, Bx = 10 G, and By = 25 G as seen at y = 0 in the xz plane.

To transfer to the chip, we move the location of the trap vertically by increasing the y bias. We also have to adjust the x bias to reduce the trap bottom. Figures 17 and 18 show the magnetic trap obtained with 20 A in the external Z wire, Bx = 4 G, and By = 80 G as seen at x = 0 in the yz plane and at y = 0 in the xz plane, respectively.

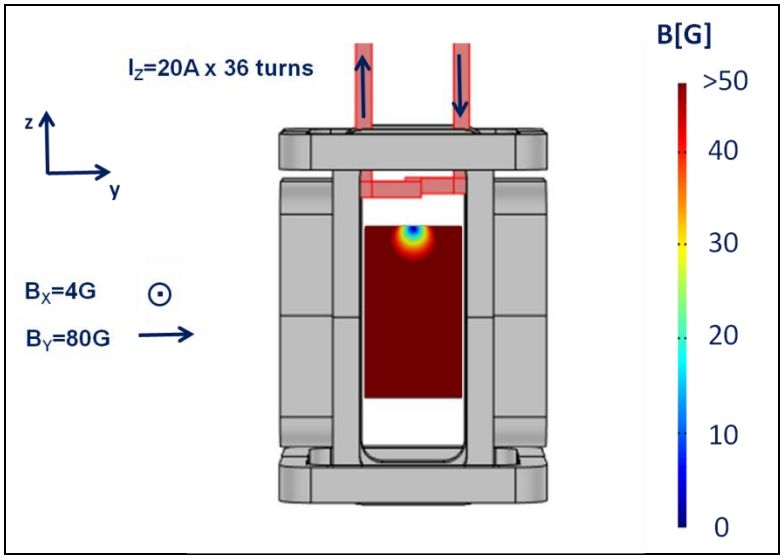

Figure 17. Magnetic field produced with a 20-A current stored in the external Z wire, Bx = 4 G, and By = 80 G as seen at x = 0 in the yz plane.

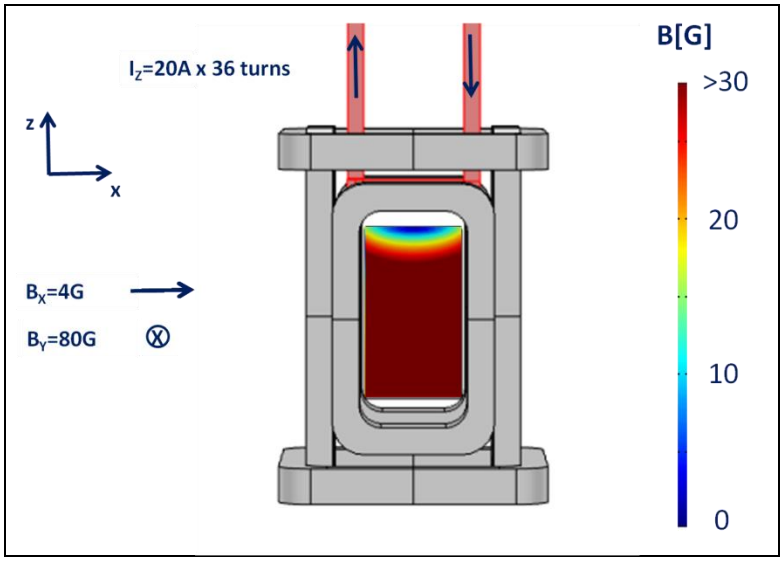

Figure 18. Magnetic field produced with a 20-A current stored in the external Z wire, Bx = 10 G, and By = 25 G as seen at y = 0 in the xz plane.

Note that the same magnetic trap location but a different strength can be obtained with 10 A in the external Z wire, Bx = 2 G, and By = 40 G as seen at x = 0 in the yz plane in figure 19 and at y = 0 in the xz plane in figure 20, respectively.

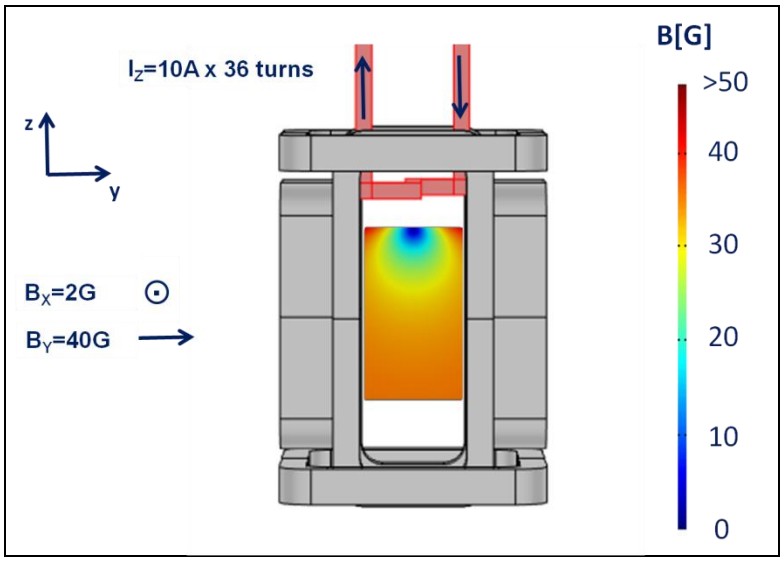

Figure 19. Magnetic field produced with a 10-A current stored in the external Z wire, Bx = 2 G, and By = 40 G as seen at x = 0 in the yz plane.

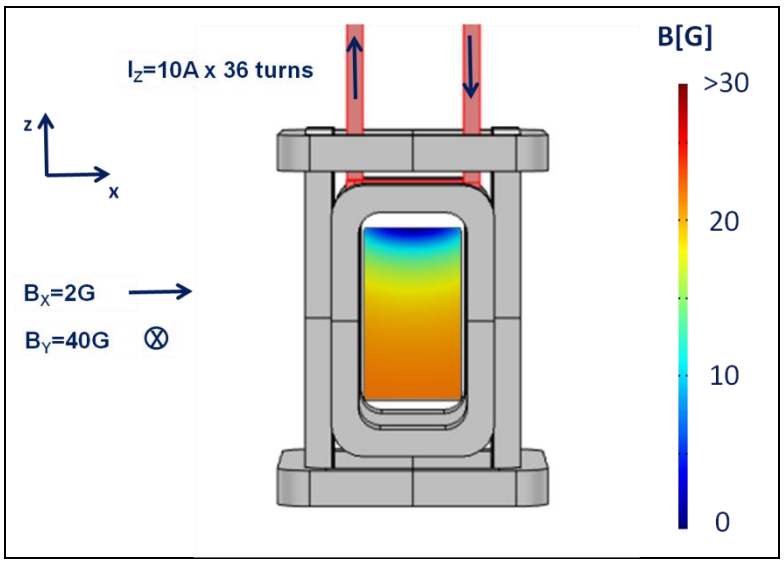

Figure 20. Magnetic field produced with a 10-A current stored in the external Z wire, Bx = 2 G, and By = 40 G as seen at y = 0 in the xz plane.

3. The Atom Chip

In our experiment, once the atoms are close to the top of the chamber, we can start the transfer to the chip. The main wire on the chip is aligned with the external Z wire and the transfer is performed by ramping down the current in the external Z wire while ramping up the current in the chip. The x and y bias fields are adjusted accordingly during the ramp. We use COMSOL to

guide us for this transfer, as well as analyze in more detail the currents and the magnetic fields on the chip. We also use COMSOL to predict the splitting of the cloud to be used for atom interferometry.

3.1 Current Density Distribution

We simulate in COMSOL the currents we apply to the atom chip in our actual experiment. The data provide a very useful tool for future chip design. Our most common current configurations are (1) the Z wire (waveguide) trap, in which we have a current flowing along the waveguide, and (2) the Dimple trap, in which we have the waveguide current, in addition to a smaller current perpendicular to the waveguide. Figure 21 shows the current density distributions corresponding to these two configurations. The Z wire trap is produced with a waveguide current I_Z = 2.5 A (left top) and a Dimple trap has the additional Dimple current of I_D = 1.5 A (right top). The zoomed sections at the bottom show the distortion (caused by the modified boundary conditions) that can occur at simple wire junctions. Even when no current is applied to the cross wires, current density variations at the junctions could deform the waveguide locally. For reference purposes, the wires are 100 and 50 µm wide in the thinnest part and 750 µm in the thickest and 10 µm thick (above the plane of vision).

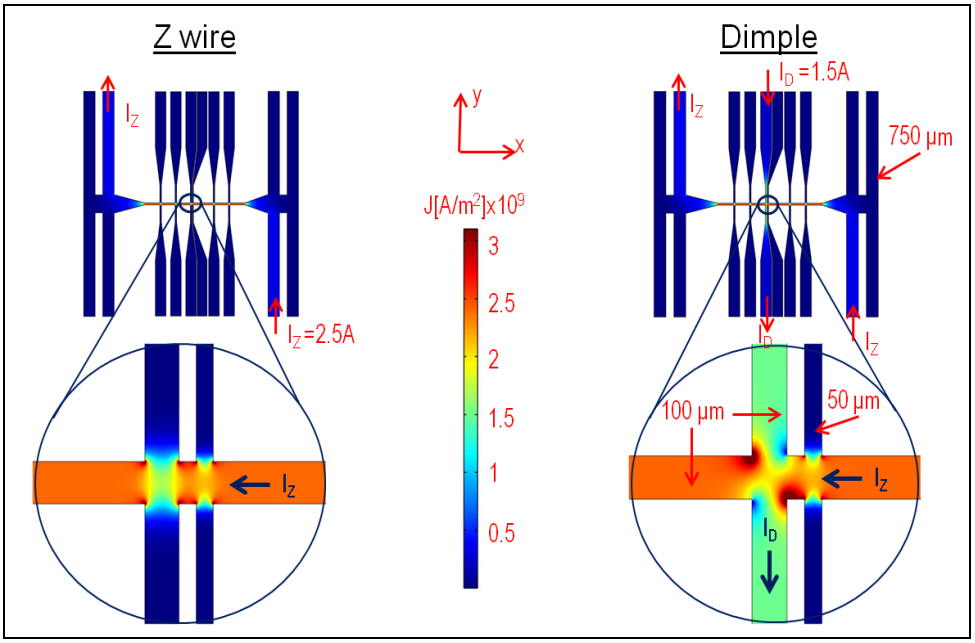

Figure 21. Current density distribution in the Z wire (waveguide) trap (top left) for a waveguide current I_Z = 2.5 A and in the Dimple trap (top right) for a Z wire current of I_Z = 2.5 A and a Dimple current of I_D = 1.5 A. The zoomed-in sections at the bottom show the distortion (caused by the modified boundary conditions) that can occur at simple wire junctions.

3.2 Magnetic Field

We use COMSOL to model the magnetic field. Figure 22 shows the magnetic field for the previously mentioned current configurations on a plane 70 µm below the chip, where the

magnetic field minimum is located. The minimum is shown in blue, as the scale indicates, and shows how the atoms will be collected. The dimple chip is used to get a very tight confinement.

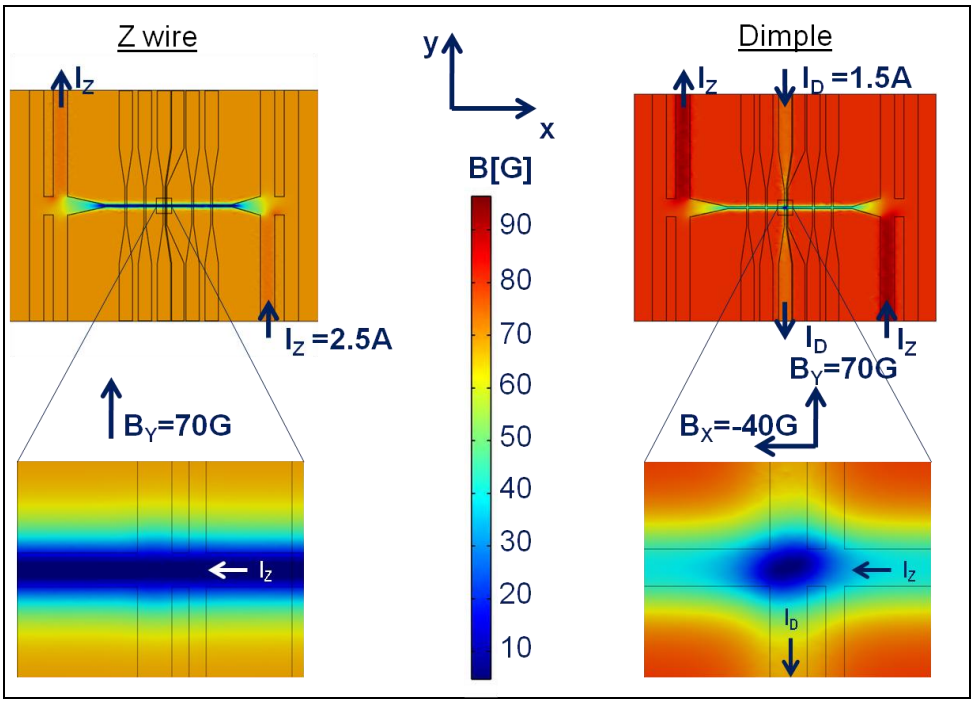

Figure 22. Magnetic field on a plane 70 μm below the chip in the Z wire (waveguide) trap (left) for a Z wire current I_Z = 2.5 A and a y bias field By = 70 G and in the Dimple trap (right) for a Z wire current I_Z = 2.5 A, a Dimple current of I_D = 1.5 A, a y bias field By = 70 G, and an x bias field Bx = –40 G.

We use LiveAtom to calculate the trap parameters. In particular, this dimple is located at (0,0,–70) μm. The magnetic field at the bottom of the trap is 0.75 G and the depth of the trap is 82.55 G. This corresponds to frequencies of (ν_x=1012, ν_y=17557, ν_z=17582) Hz. The trap gradient is very sensitive to small variations in the field and current. The trap position varies with the magnetic field variations; for instance, a 1-μm position corresponds to a 2% fluctuation in the By magnetic field variation, and up to 6% of the Bx magnetic field, up to 2% of field due to the external Z wire, and up to 10% of the dimple current.

3.3 Splitting the Cloud

With our current chip, we have various wire paths and we can combine different current configurations with various external bias fields that can offer the means to create well-controlled and repeatable coherent splitting of the atomic cloud through dynamically adjusting the currents and bias fields. For instance, figure 23 shows something very similar to the Dimple trap, except that current is being sent through two adjacent wires, something like a small Z wire trap inside the Z wire trap. If we zoom in the area at the center, we can see the fields better. Figure 24 shows the expanded region of figure 23.

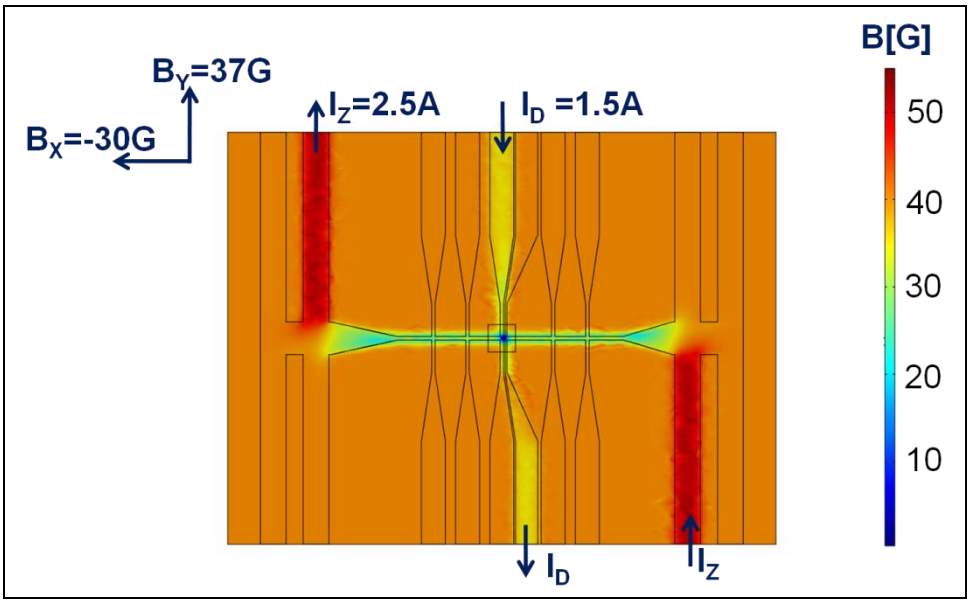

Figure 23. Magnetic field on a plane 70 µm below the chip in the mini Z trap for a Z wire current I_Z = 2.5 A, a Mini Z current of I_D = 1.5 A, a y bias field By = 37 G, and an x bias field Bx = –30 G.

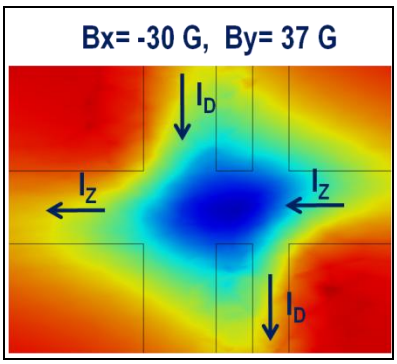

Figure 24. Center of figure 22, expanded. Magnetic field on a plane 70 µm below the chip in the mini Z trap for a Z wire current I_Z = 2.5 A flowing to the left, a mini Z current of I_D = 1.5 A, flowing down, then to the left, then down, a y bias field By = 37 G, and an x bias field Bx = –30 G.

By varying the fields, we can stretch the potential minima. By increasing the magnitude of the field along x while decreasing it along y, we can stretch the cloud along y. Increasing the field in the opposite direction, we can actually split the cloud. Figure 25 shows the magnetic field in a plane 70 µm below the chip for different values of the x and y bias fields. In both cases, the ratio and magnitude of the bias fields are varied while keeping the currents constant in such a way that the trap bottom is still at 70 µm below the chip. It is important to note that coherently splitting with magnetic fields requires precise control of the magnetic fields, or a smooth change of the magnetic fields.

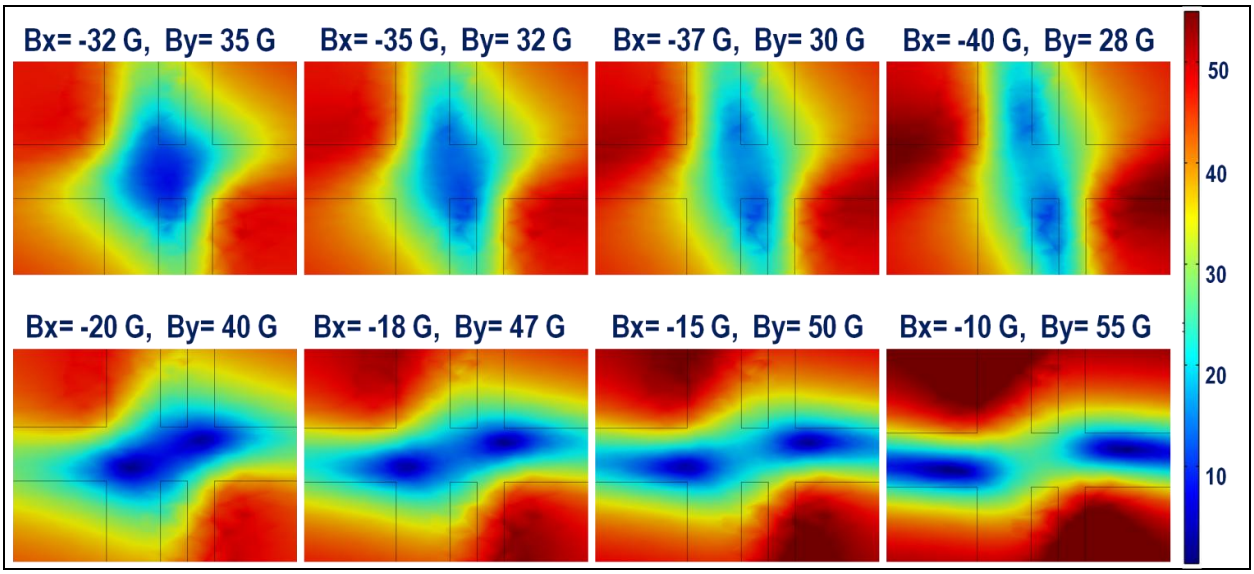

Figure 25. Magnetic field on a plane 70 µm below the chip in the mini Z trap for a Z wire current I_Z = 2.5 A flowing to the left, and a mini Z current of I_D = 1.5 A, flowing down, then to the left, then down. Increasing the ratio $|B_x|/B_y$ stretches the cloud along y, while decreasing the ratio $|B_x|/B_y$ splits the cloud along x.

4. Exotic Geometries

In figure 26, we have a simulation of a different wire geometry, useful for new chip designs (knowing what to do and what not to do depending on the purpose of the chip), or a more detailed view of exactly what happens near wire junctions. The top picture represents the magnetic field at 15 µm below the geometry for a 100-µm-wide and 10-µm-thick wire with a 100 µm x 100 µm pivot when a 1-A current is sent through it with a 70-G magnetic field. The bottom picture represents the side view of the magnetic fields due to that wire.

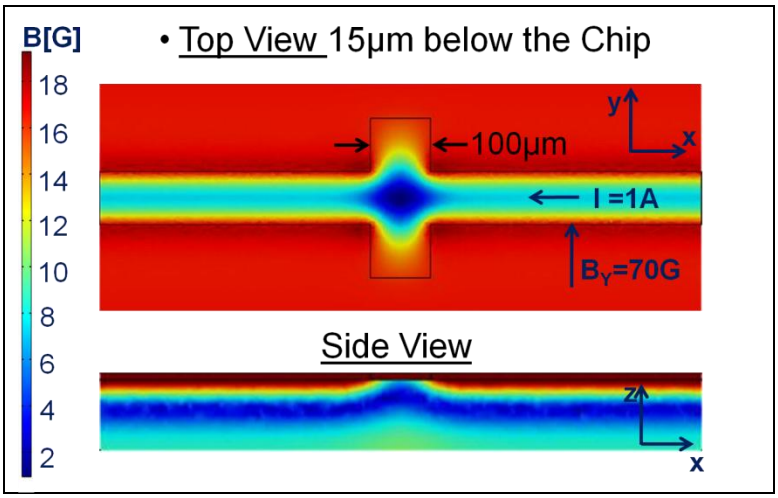

Figure 26. Magnetic field at 15 μm below the geometry for a 100-μm-wide and 10-μm-thick wire with a 100 μm x 100 μm pivot when a 1-A current is sent through it with a 70-G magnetic field.

In figure 27, we have a collection of pivots like the one before, separated by 500 μm from each other. If we were to transport atoms through such waveguide, we would be changing the gravitational potential of the atoms each time they pass under a pivot. The last (bottom) picture represents the current density distribution due to 1 A flowing through the geometry.

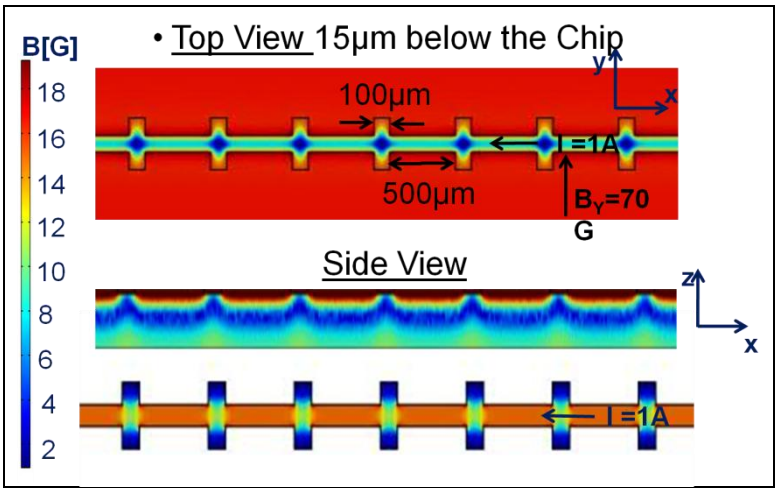

Figure 27. Magnetic field at 15 μm below the geometry for a collection of pivots 100 μm wide and 10 μm thick with a 100 μm x 100 μm pivot when a 1-A current is sent through it with a 70-G magnetic field.

Figure 28 shows yet another possible geometry and the corresponding current density distribution on the top and the magnetic field below the chip on the bottom. As we round the edges of the holes, we can change the current density and smooth the magnetic field, as seen in the frames on the right.

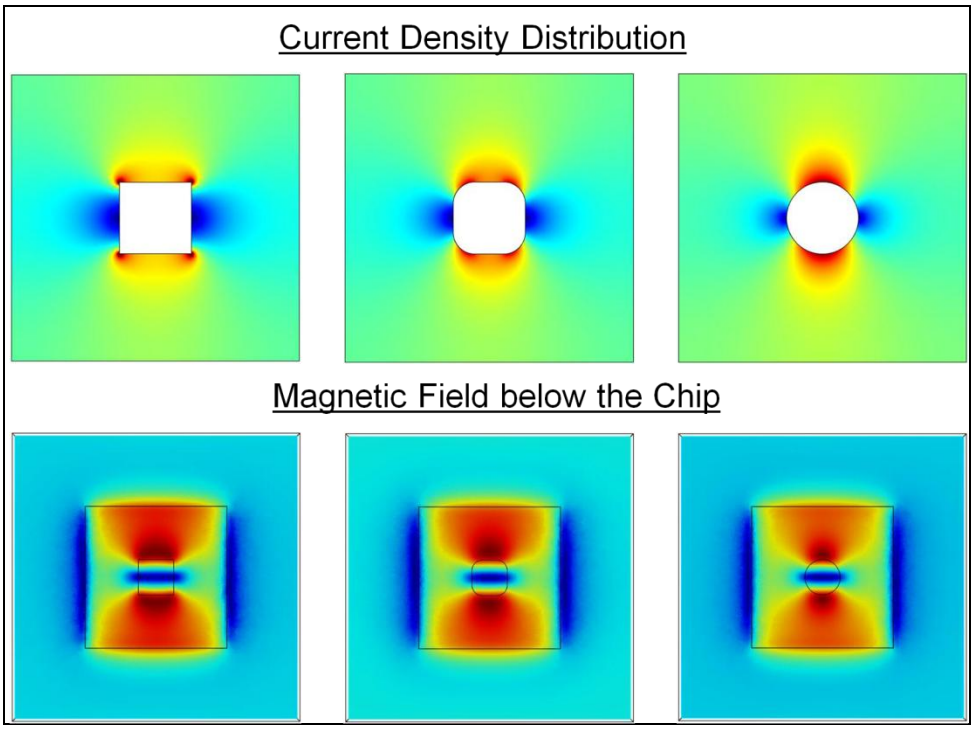

Figure 28. Magnetic field at 15 μm below the geometry for a collection of pivots 100 μm wide and 10 μm thick with a 100 μm x 100 μm pivot when a 1-A current is sent through it with a 70-G magnetic field

5. Conclusions

In this report, we have provided an overview of the computer simulations we have performed using COMSOL and LiveAtom and how we use them to predict experimental parameters. These simulations are useful not only to guide us through our experimental procedure, but also to estimate and predict potential thermal issues, as well as design new chips.

6. References

1. COMSOL. http://www.comsol.com/ (accessed March 2013).
2. LiveAtom. http://www.boulderlabs.com/liveatom/ (accessed March 2013).
3. McGuirk, J. M.; Foster, G. T.; Fixler, J. B.; Snadden, M. J.; Kasevich, M. A. Sensitive Absolute-Gravity Gradiometry Using Atom Interferometry, *Phys. Rev. A* **2002**, *65*, 033608.
4. Andrews, M. R.; Townsend, C. G.; Miesner, H.-J.; Durfee, D. S.; Kurn, D. M.; Ketterle, W. Observation of Interference Between Two Condensates, *Science* **1997** *275*, 637.
5. Schumm, T.; Hofferberth, S.; Andersson, L. M.; Wildermuth, S.; Groth, S.; Bar-Joseph, I.; Schmiedmayer, J.; Kruger. P. Matter-Wave Interferometery in a Double Well on an Atom Chip, *Nature Physics* **2005**, *1*, 57–62.
6. Hofferberth, S.; Lesanovsky, I.; Fischer, B.; Verdu, J.; Schmiedmayer, J. Radiofrequency-Dressed-State Potentials for Neutral Atoms, *Nature Physics* **2006**, *2*, 710.
7. Jo, G.-B.; Choi, J.-H.; Christensen, C. A.; Pasquini, T. A.; Lee, Y.-R.; Ketterle, W.; Pritchard, D. E. Phase-Sensitive Recombination of Two Bose-Einstein Condensates on an Atom Chip, *Phys. Rev. Lett.***2007**, *98*, 030407.
8. Lesanovsky, I.; Schumm, T.; Hofferberth, S.; Andersson, L. M.; Krüger, P.; Schmiedmayer, J. Adiabatic Radio-Frequency Potentials for the Coherent Manipulation of Matter Waves, *Phys. Rev. A* **2006**, *73*, 033619.
9. Hänsel, W.; Hommelhoff, P.; Hänsch, T. W.; Reichel, J. Bose-Einstein Condensation on a Microelectronic Chip, *Nature* **2001**, *413*, 498.
10. Ott, H.; Fortagh, J.; Schlotterbeck, G.; Grossmann, A.; Zimmermann, C. Bose-Einstein Condensation in a Surface Microtrap *Phys. Rev. Lett.* **2001**, *87*, 230401.
11. Kasevich, M. Coherence with Atoms, *Science* **2002**, *298*,1363.
12. ColdQuanta. Products. http://www.coldquanta.com/Products__BEC_%26_Ultra-cold.html (accessed March 2013).
13. Farkas, D. M.; Hudek, K. M.; Salim, E. A.; Segal, S. R.; Squires, M. B.; Anderson, D.Z.A Compact, Transportable, Microchip-Based System for High Repetition Rateproduction of Bose-Einstein Condensates, *Appl. Phys. Lett* **2010**, *96*, 093102.
14. Alexander, J.; Rowlett, C.; Prieto, V.; Golding, W.; Lee, P. *Experiments in Cold Atom Optics at the Army Research Laboratory I: Experimental Set-up*; ARL-TR-5787; U.S. Army Research Laboratory: Adelphi, MD, 2011.

1 (PDF)	DEFENSE TECHNICAL INFORMATION CTR DTIC OCA
1 (PDF)	DIRECTOR US ARMY RESEARCH LAB RDRL CIO LL
1 (PDF)	GOVT PRINTG OFC A MALHOTRA
8 (PDF)	DIRECTOR US ARMY RESEARCH LAB ATTN RDRL SEE I VIOLETA PRIETO JASON ALEXANDER WILLIAM GOLDING PATRICIA LEE DORAN SMITH PARVEZ UPPAL ATTN RDRL SEE GARY WOOD PATTI GILLESPIE

INTENTIONALLY LEFT BLANK.